IEEE Access
Multidisciplinary | Rapid Review | Open Access Journal

IEEE SYSTEMS, MAN AND CYBERNETICS SOCIETY SECTION

Received 9 August 2023, accepted 31 August 2023, date of publication 11 September 2023, date of current version 19 September 2023.

Digital Object Identifier 10.1109/ACCESS.2023.3314382

APPLIED RESEARCH

Dynamic Sliding Mode Control With PID Surface for Trajectory Tracking of a Multirotor Aircraft

JOVANI ORTEGA VENTURA[1], DANIEL BENITEZ MORALES[1], JESUS P. ORDAZ OLIVER[1], AND EDUARDO S. ESPINOZA QUESADA[2], (Senior Member, IEEE)

[1]CITIS, AACyE, ICBI, Universidad Autónoma del Estado de Hidalgo, Hidalgo 42184, México
[2]CONACYT-CINVESTAV, UMI-LAFMIA, México City 07360, Mexico

Corresponding author: Eduardo S. Espinoza Quesada (eduardo.espinoza@cinvestav.mx)

This work was supported in by the UAEH Doctorado en Ciencias en Automatización y Control, and in part by the Consejo Nacional de Humanidades, Ciencias y Tecnologías (CONAHCYT).

ABSTRACT This paper deals with the design of a robust controller to attenuate matched and unmatched uncertain dynamics as well as external disturbances effects by considering the actuator bandwidth to stabilize the mechanical dynamics of an Unmanned Aerial Vehicle. To this end, the performance of a sliding mode controller is improved with the combination of the attractive ellipsoid method. Likewise, it is guaranteed that the system trajectory arrives into a minimal size invariant set in finite time by using a workable control input. Finally, in order to evaluate the effectiveness of the proposed control approach, a comparative study with a robust Proportional Derivative controller, an integral sliding mode controller and a dynamic sliding mode controller with Proportional Integral Derivative sliding surface was conducted. In order to validate the effectiveness of the proposed controllers, the dynamics of a multirotor aircraft was used to conduct numerical simulations.

INDEX TERMS UAV, uniformly ultimately bounded stability, sliding mode control, PID surface.

I. INTRODUCTION

An Unmanned Aerial Vehicle (UAV) is an underactuated nonlinear system that has been used in commercial, industrial, military and civil applications [1], [2], [3]. This is due to its versatility for conducting hover flight and trajectory tracking [4], [5]. Commonly, this class of aircraft system is driven by rotors and stabilized via a linear controller for indoors and outdoors applications [6], [7], [8], [9]. Traditionally, the stabilization of a UAV is performed via Proportional Derivative (PD) controllers and tuned via linear quadratic regulator algorithms [10]. Also, new techniques are used to stabilize UAV like a model predictive controller that uses a linearized UAV model and an observer to measure the external disturbance which are going to be compensated and the predictive controller improves the performance of a quadcopter [11], another one, quaternion-based tracking controller to stabilize a UAV but it does not deal with external disturbance [12]. Robust control for stabilization of this underactuated system type has been also used in [13] to demonstrate the advantages of a dynamic sliding mode control and attractive ellipsoid method to reduce perturbation effects. Recently, robust control of a UAV has attract the attention on advanced mobile robots field because they are sensitive to external disturbances in outdoor flights, actually, the reduction of unmatched disturbances effects is one of the main challenges of this kind of systems. In fact, disturbance and uncertainty rejection is a major objective in control system design. Indeed, for underactuated controlled systems this issue degrades the trajectory tracking performance such that in some cases it is not possible to conclude stability in the Lyapunov sense [3], [6]. Nowadays, different robust controllers are designed to reduce these effects, even under the most extreme situations. This is the case of the Sliding Mode Control (SMC), the robust control based on Attractive ellipsoid Method (AEM), and neural networks, see for example [1], [14], [15], and [16].

The control problem can be associated with UAV regulation problem in the presence of disturbances for trajectory tracking. The most interesting features of sliding mode control are insensitivity, reduction of the unmatched disturbances and uncertain dynamics, as well as finite-time convergence to the sliding surface [15], [17]. However, a drawback of the controllers based on the sliding mode

The associate editor coordinating the review of this manuscript and approving it for publication was Xiaojie Su.

technique is the chattering effect on the actuator [18], [19]. This phenomenon represents a complex closed-loop control problem and in some situations, this one cannot be reliably realized in practice [17], [20]. In recent years, researchers have managed how to attenuate the chattering effect and preserve robust control properties by proposing controllers like dynamic sliding mode, adaptive sliding mode, high order sliding mode, some variations of fuzzy and neural network-based control, and other variable structure controls [21], [22], [23], [24], [25], [26], [27], [28], [29].

Other effective approach for reducing external disturbances and uncertain dynamics effects in control systems is the robust control based on AEM-concept. This strategy uses a linear feedback control employing fixed gain. In fact, under a suitable gain tuning, this control approach provides robustness property to considerably reduce both uncertain dynamics as well as external disturbances effects [14], [30]. The aim of AEM is, by using linear or non linear feedback control, to enclose the trajectories of the disturbed system into a small size invariant region. Although this approach implies that system trajectories arrive into a small size multi-dimensional ellipsoid, this one is valid only in some region of attraction. Actually, in some cases, the obtained control gain results in the actuator wear. Recently, the controllers based on the sliding motion was further improved by introducing the properties of the AEM-concept [13], [24], [27].

The AEM presents an effect called high-gain effect [27] that is not desired because it can amplify the noise of the system with a high gain of the controller, and also, the energy consumption [31]. On the other hand, SMCs present chattering, which is an undesirable phenomenon and it is perceived as oscillations with finite frequency and amplitude. The chattering effects are related to low control accuracy and high wear of moving mechanical parts [18]. In order to reduce such chattering effects, in this paper we present a class of dynamic control consisting in the incorporation of the proportional, integral, and derivative of the adjoint sliding surface. Furthermore, since the sliding surface is a second-order system of the adjoint variable, a workable control signal is obtained. Getting as the major contribution Ultimate Uniform Bound Stability (UUB-Stability) for nonlinear systems without exact knowledge of the dynamic model equations and in the presence of external bounded disturbances. Finally, in order to demonstrate the effectiveness of the designed controller, a comparative study of the implementation of integral sliding mode control and proportional derivative control to the dynamics on a multirotor unmanned aircraft system is presented. The main contributions of this work are summarized as follows:

- By using the Newton-Euler approach a mathematical model of a home made non conventional hexarotor is derived.
- The control action to regulate orientation and guarantee the trajectory tracking of the multirotor system, which is a class of dynamic sliding mode control (DSMC) with a Proportional Integral Derivative (PID) type sliding surface is developed.
- The stability analysis to guarantee the so called Ultimate Uniform Bound Stability of the closed-loop hexarotor system is presented.

On the other hand, a comparative study is conducted to analyze the UAV performance between the proposed control, a PD control and with an integral sliding mode control (ISMC). Likewise, a comparative study based of the error signals and the energy consumption of the designed robust controller with PID and ISMC is presented. The rest of the paper is organized as follows. The system description of the multirotor aircraft, the mathematical preliminaries and the problem formulation are introduced in Section II and Section III, respectively. The robust control design for a class of uncertain disturbed linear systems is presented in Section IV. The illustrative scenario of the multirotor system regulation inspired on a tracking trajectory task is presented in Section V. Finally, in Section VI concluding remarks are presented.

II. SYSTEM DESCRIPTION

The schematic structure of the multirotor system is illustrated in Figure 1 which is an aircraft that consists of six rotors. In order to describe the UAV motion, two reference frames are necessary: the earth inertial frame (X_I, Y_I, Z_I) and the body-fixed frame (X_B, Y_B, Z_B). The sum of the forces of each rotor (f_1, f_2, f_3, f_4, f_5, f_6) generates the thrust force and is oriented parallel to the Z_B axis. Let $\bar{q} = (\Gamma, \eta)$ be the generalized coordinates of the system, where $\Gamma = (x(t), y(t), z(t))^\intercal$ represents the translation coordinates relative to the inertial frame and $\eta = (\phi(t), \theta(t), \psi(t))^\intercal$ is the vector of the Euler angles that represents the attitude of the vehicle. Now, the transformation from the body frame to the inertial frame is realized by using the rotation orthogonal matrix ($\mathcal{R}$). In addition, the angular velocities in the body frame can be expressed in terms of the Euler angle velocities by using the corresponding rotation matrix W_η. This procedure is described for example in [32], [33], and [34].

A. THE HEXAROTOR AIRCRAFT DYNAMICS

The equations of motion of the aircraft obtained by using the Newton-Euler formalism whose equations describe the translational and rotational movements are given as [35], [36], and [37]:

$$\begin{aligned} \dot{\Gamma} &= V \\ m\dot{V} &= \mathcal{R}F \\ \dot{\mathcal{R}} &= \mathcal{R}\hat{\Omega} \\ I\dot{\Omega} &= -\Omega \times I\Omega + \tau, \end{aligned} \tag{1}$$

where $F = \begin{bmatrix} 0 & 0 & u_z(t) \end{bmatrix}^\intercal + \mathcal{R}^\intercal \begin{bmatrix} 0 & 0 & -mg \end{bmatrix}^\intercal$ and $\tau = \begin{bmatrix} \tau_\phi(t) & \tau_\theta(t) & \tau_\psi(t) \end{bmatrix}^\intercal$ are the total forces and moments acting on the UAV, respectively. $V = (\dot{x}(t), \dot{y}(t), \dot{z}(t))^\intercal \in \mathbb{R}^3$ is the translational speed with respect to the inertial frame and $\hat{\Omega}$

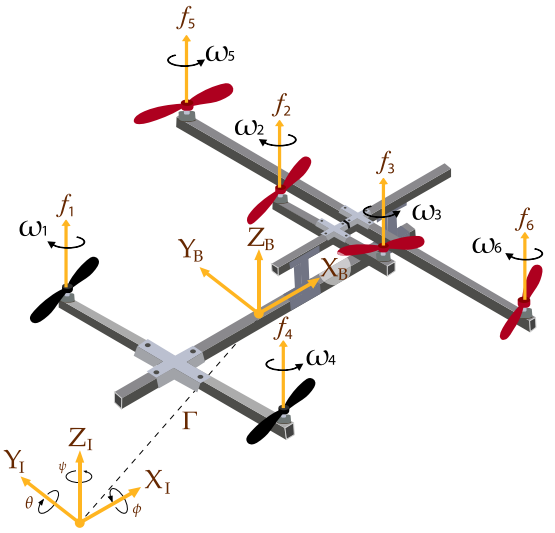

FIGURE 1. Configuration of the hexarotor UAV.

is a skew-symmetric matrix such that $\hat{\Omega} = \Omega \times a$. The Ω term is the vector of angular velocities in the body frame, m denotes the mass of the UAV and I contains the moments of inertia about the center of mass. Then, applying relation (1), the dynamic equations of the aircraft can be expressed as follows:

$$\begin{aligned}
\ddot{x}(t) &= \frac{1}{m}\left[(c\phi(t)s\theta(t)c\psi(t) + s\phi(t)\, s\psi(t))u_z(t)\right] + \xi_x(t),\\
\ddot{y}(t) &= \frac{1}{m}\left[(c\phi(t)s\theta(t)s\psi(t) - s\phi(t)c\psi(t))u_z(t)\right] + \xi_y(t),\\
\ddot{z}(t) &= \frac{1}{m}\left[(c\phi(t)c\theta(t))u_z(t)\right] - g + \xi_z(t),\\
\ddot{\phi}(t) &= \frac{I_{zz}}{a_1}\left[a_2 + \tau_\phi(t)\right] - \frac{I_{xz}}{a_1}\left[a_3 + \tau_\psi(t)\right] + \xi_\phi(t),\\
\ddot{\theta}(t) &= \frac{1}{I_{yy}}\left[a_4 - \dot{\psi}(t)\dot{\psi}(t)I_{xz} + \tau_\theta(t)\right] + \xi_\theta(t),\\
\ddot{\psi}(t) &= \frac{I_{xx}}{a_1}\left[a_3 + \tau_\psi(t)\right] - \frac{I_{zx}}{a_1}\left[a_2 + \tau_\phi(t)\right] + \xi_\psi(t).
\end{aligned} \tag{2}$$

where for shortness cos $\rightarrow c$, sin $\rightarrow s$, and

$$\begin{aligned}
a_1 &= (I_{xx}I_{zz} - I_{xz}I_{zx}),\\
a_2 &= \dot{\theta}(t)\left(\dot{\psi}(t)I_{yy} - \dot{\phi}(t)I_{zx} - \dot{\psi}(t)I_{zz}\right),\\
a_3 &= \dot{\theta}(t)\left(\dot{\psi}(t)I_{xz} + \dot{\phi}(t)I_{xx} - \dot{\phi}(t)I_{yy}\right),\\
a_4 &= \dot{\phi}(t)\left(\dot{\phi}(t)I_{zx} + \dot{\psi}(t)I_{zz} - \dot{\psi}(t)I_{xx}\right).
\end{aligned} \tag{3}$$

$\xi_x(t)$, $\xi_y(t)$, $\xi_z(t)$, $\xi_\phi(t)$, $\xi_\theta(t)$ and $\xi_\psi(t)$ denote the uncertainties, unmodeled dynamics and external disturbances. $\tau_\phi(t)$,$\tau_\theta(t)$ and $\tau_\psi(t)$ are the torques that generate the roll, pitch and yaw movements. The input u_z is associated with the forces generated by the six rotors. For this aircraft the following assumptions were considered:

- The center of mass of the vehicle coincides with the origin of the body frame.
- At low speeds, the aerodynamic effects can be neglected.
- Angular velocities respect to the body frame and inertial frame are the same for low speeds.
- The propellers are rigid with fixed pitch.
- The aircraft doesn't make aggressive maneuvers, then $-\frac{\pi}{2} < \phi < \frac{\pi}{2}$ and $-\frac{\pi}{2} < \theta < \frac{\pi}{2}$.

III. MATHEMATICAL PRELIMINARIES AND PROBLEM FORMULATION

Consider the uncertain nonlinear system affine in the control

$$\begin{aligned}
&\dot{\bar{x}}(t) = \mathbf{A}\bar{x}(t) + \mathbf{B}u(t) + \xi(t),\\
&\bar{x}(0) = \bar{x}_0,\ \xi(t) = f(\bar{x}) + g(\bar{x})u(t) - \mathbf{A}\bar{x}(t) - \mathbf{B}u(t) + \Delta(t)
\end{aligned} \tag{4}$$

where $\bar{x}(t) \in \mathbb{R}^n$ at time $t \in \mathbb{R}$. The $n \times n$ matrix $\mathbf{A}$ is the state matrix associated with the linear system representation $\bar{x}(t)$. The control input is given by $u(t) \in \mathbb{R}^m$, and $\mathbf{A}$, $\mathbf{B}$ are known real constant matrices with appropriate dimensions, furthermore, it is assumed that the pair $(\mathbf{A}, \mathbf{B})$ is controllable, the vector functions $f : \mathbb{R}^n \rightarrow \mathbb{R}^n$ and $g : \mathbb{R}^n \rightarrow \mathbb{R}^p$ define the dynamics mapping of system (4). $\mathbf{B} \in \mathbb{R}^{n\times m}$ is the matrix realizing the actuator-mapping, and $\Delta(t)$ are external disturbances in $\mathbb{R}^n$. System uncertainties and external disturbances are denoted as $\xi \in \mathbb{R}^n$.

Assumption 1: The uncertain term of the considered system as well as its variations satisfies the following condition

$$\|\xi(t)\| \leq \delta_1,\ \|\dot{\xi}(t)\| \leq \delta_2,\ 0 < \delta_1 < \infty,\ 0 < \delta_2 < \infty, \tag{5}$$

where $\|\cdot\|$ denotes the standard Euclidean norm.

To represent the nominal system in two subsystems (the one associated with the control signal and the one non associated) the transformation $z = \mathbf{T}\bar{x}$ is applied, where $\mathbf{T} \in \mathbb{R}^{n\times n}$ is given as:

$$\mathbf{T} = \left[\mathbf{N_B}\ \mathbf{B}\right]^\intercal, \tag{6}$$

with $\mathbf{N_B} \in \mathbb{R}^{(n-m)\times m}$ the null-space of the output matrix $\mathbf{B}^\intercal$. Thus, system (4) can be rewritten in the new system representation as:

$$\dot{z}(t) = \mathcal{A}z(t) + \mathcal{B}u(t) + \bar{\xi}(z,t),\quad z(0) = \mathbf{T}x_0, \tag{7}$$

where $\mathcal{A} = \mathbf{TAT}^{-1} \in \mathbb{R}^{n\times n}$, $\mathcal{B} = \mathbf{TB} \in \mathbb{R}^{n\times m}$ and $\bar{\xi} = \mathbf{T}\xi(z,t) \in \mathbb{R}^n$. Here, it is assumed that system (7) contains matched and unmatched nonvanishing uncertainties, where their adverse effects may not be mitigated with any control action. To reduce this effects, consider a PID type sliding surface $\Phi(t) : \mathbb{R}^m \rightarrow \mathbb{R}^m$ as:

$$\Phi(t) = \mathbf{K}_1\varphi(t) + \mathbf{K}_2\int_{t_0}^{t}\varphi(\tau)d\tau + \mathbf{K}_3\dot{\varphi}(t) \tag{8}$$

where $\varphi \in \mathbb{R}^m$ is the adjoint sliding variable defined as $\varphi = z_2 + \mathbf{R}z_1$ where $z_1 \in \mathbb{R}^{(n-m)}$ and $z_2 \in \mathbb{R}^m$, the m by m diagonal matrices $(\mathbf{K}_1,\ \mathbf{K}_2\ \mathbf{K}_3)$ and $\mathbf{R} \in \mathbb{R}^{m\times(n-m)}$ are adjustment matrices. Here, the control problem statement is divided in two stages. The first one consist in obtaining an admissible control signal u such that the adjoint variable σ arrives to

the invariant set $\Upsilon = \{z(t) \in \mathbb{R}^n : \|\varphi(t)\| \leq \delta, \forall\, t \geq T_2\}$, for small as possible $0 < \delta$. The second stage consist in obtaining the gain matrices ($\mathbf{K}_1$, $\mathbf{K}_2$, $\mathbf{K}_3$, $\mathbf{R}$) such that the effects of the non-vanishing uncertainties and disturbances are reduced. This problem is studied using the concept of UUB-Stability.

To achieve the problem statement goal, the following concepts are employed:

Definition 1 (Attractive ellipsoid [14]): The ellipsoid

$$\mathcal{E}\left(0, \bar{\boldsymbol{P}}^{-1}\right) = \{\bar{x}(t) \in \mathbb{R}^n : \bar{x}(t)^{\mathsf{T}}\bar{\boldsymbol{P}}\bar{x}(t) \leq 1,\ \bar{\boldsymbol{P}} = \bar{\boldsymbol{P}}^{\mathsf{T}}\}, \quad (9)$$

with center at the origin and the corresponding non-degenerated ellipsoidal matrix $\bar{\boldsymbol{P}}$, is attractive for some dynamic system if for any trajectory $\{\bar{x}(t)\}_{t\geq 0}$ the following property holds:

$$\limsup_{t\to\infty} \bar{x}^{\mathsf{T}}(t)\bar{\boldsymbol{P}}\bar{x}(t) \leq 1. \quad (10)$$

Definition 2 (UUB-Stability [38]): The nonlinear dynamical system $\dot{\bar{x}}(t) = f(t, \bar{x}(t)),\ \bar{x}(t_0) = \bar{x}_0,\ t \geq t_0$ is Ultimately Uniformly Bounded with bound b if there exists some $a \in (0, c)$ such that:

$$\|\bar{x}(t_0)\| \leq a,\ \Longrightarrow\ \|\bar{x}(t)\| \leq b,\ \forall\, t \geq t_0 + T$$

for positive $b, c \in \mathbb{R}$ and $T = T(a, b)$ independent of t_0.

Proposition 1 (On the attractive set [14]): Let a real valued function $V : \mathbb{R}^n \to \mathbb{R}$, satisfying

$$\dot{V}(z(t)) \leq -\alpha V(z(t)) + \beta,\ z(t) \in \mathbb{R}^n, \quad (11)$$

for positive scalars α and β, then $V(z(t))$ is an attractive set, furthermore

$$\limsup_{t\to\infty} V(z(t)) \leq \frac{\beta}{\alpha},\ \text{is fulfilled.} \quad (12)$$

Thus, the problem associated with the hexarotor system consists of finding sufficient conditions such that the proposed control guarantees UUB-stability of the closed-loop system. Also, the control law must regulate the orientation of the aircraft and guarantee robust trajectory tracking in the $x(t)$, $y(t)$, $z(t)$ space even with disturbances or uncertainties. On the other hand, after a finite time, the control law drives the system trajectories to a minimal size attractive ellipsoid in exponential form.

IV. ROBUST CONTROL DESIGN

Noticed that system (7) can be rewritten as:

$$\begin{aligned}
\dot{z}_1(t) &= \mathcal{A}_{11}z_1(t) + \mathcal{A}_{12}z_2(t) + \bar{\xi}_1(z, t),\\
z_1(0) &= z_1^0,\\
\dot{z}_2(t) &= \mathcal{A}_{21}z_1(t) + \mathcal{A}_{22}z_2(t) + \bar{\xi}_2(z, t) + \mathcal{B}_2u(t),\\
z_2(0) &= z_2^0,
\end{aligned} \quad (13)$$

where $\mathcal{A}_{11} \in \mathbb{R}^{(n-m)\times(n-m)}$, $\mathcal{A}_{12} \in \mathbb{R}^{(n-m)\times m}$, $\mathcal{A}_{21} \in \mathbb{R}^{m\times(n-m)}$, $\mathcal{A}_{22} \in \mathbb{R}^{m\times m}$, and $\mathcal{B}_2 \in \mathbb{R}^{m\times m}$. Based on the fact, that the pair $(\mathcal{A}, \mathcal{B})$ is controllable, it is evident to verify that the pair $(\mathcal{A}_{11}, \mathcal{A}_{12})$ is also controllable.

Proposition 2: If the dynamic of the control action associated to system (13) is given by

$$\begin{aligned}
\dot{u}(t) = -\mathcal{B}_2^{-1}\mathbf{K}_3^{-1}\{&(\mathbf{K}_3\{\mathbf{Q}_1\mathcal{A}_{11} + \mathbf{Q}_2\mathcal{A}_{21}\} + \mathbf{K}_1\mathbf{Q}_1)\, z_1(t)\\
&+ (\mathbf{K}_3\{\mathbf{Q}_1\mathcal{A}_{12} + \mathbf{Q}_2\mathcal{A}_{22}\} + \mathbf{K}_2 + \mathbf{K}_1\mathbf{Q}_2)\, z_2(t)\\
&+ (\mathbf{K}_3\mathbf{Q}_2\mathcal{B}_2 + \mathbf{K}_1\mathcal{B}_2)\, u(t) + \boldsymbol{\rho}\,\mathrm{sign}(\Phi(t))\},\\
\mathrm{Sign}(\Phi(t)) = &\begin{bmatrix} \mathrm{sign}(\Phi_1(t)) \\ \vdots \\ \mathrm{sign}(\Phi_m(t)) \end{bmatrix},\ u(0) = 0,
\end{aligned} \quad (14)$$

where $\mathbf{Q}_1 = (\mathcal{A}_{21} + \mathbf{R}\mathcal{A}_{11})$, $\mathbf{Q}_2 = (\mathcal{A}_{22} + \mathbf{R}\mathcal{A}_{12})$, and $\boldsymbol{\rho} = \mathrm{diag}\,(\rho_1, \cdots, \rho_m)$ is a m by m positive definite matrix, then after time $t_r = \frac{\sqrt{2}}{\alpha_1}V^{\frac{1}{2}}(\Phi(t_0)) + t_0$, under storage function $V_1(\Phi(t)) = \sum_{i=1}^{m}\Phi_i^2(t)$, the hyperplane $\Phi(t) = \bar{0}_m$ is the sliding manifold for the sliding variable surface (8).

Proof. The control action (14) is a class of dynamic sliding mode control and when control is integrated, the chattering effect is reduced. In the following sections this control is referred as robust controller (RC). Consider the storage function $V_1(\Phi(t))$. Its time variations is given by:

$$\dot{V}_1(\Phi(t)) = \Phi^{\mathsf{T}}(t)\left(\mathbf{K}_1\dot{\varphi}(t) + \mathbf{K}_2\varphi(t) + \mathbf{K}_3\ddot{\varphi}(t)\right). \quad (15)$$

Since the first and second time derivative of adjoint variable $\varphi(t) \in \mathbb{R}^m$ along the system trajectories (13) are given by

$$\begin{aligned}
\dot{\varphi}(t) =&\mathbf{Q}_1z_1(t) + \mathbf{Q}_2z_2(t) + \left[\mathbf{R},\ \mathbf{I}_m\right]\bar{\xi}(z, t) + \mathcal{B}_2u(t),\\
\ddot{\varphi}(t) =&\{\mathbf{Q}_1\mathcal{A}_{11} + \mathbf{Q}_2\mathcal{A}_{21}\}\, z_1(t)\\
&+ \{\mathbf{Q}_1\mathcal{A}_{12} + \mathbf{Q}_2\mathcal{A}_{22}\}\, z_2(t) + [\mathbf{Q}_1,\ \mathbf{Q}_2]\,\bar{\xi}(z, t)\\
&+ \mathbf{Q}_2\mathcal{B}_2u(t) + \left[\mathbf{R},\ \mathbf{I}_m\right]\dot{\bar{\xi}}(z, t) + \mathcal{B}_2\dot{u}(t).
\end{aligned} \quad (16)$$

$\mathbf{I}_m$ defines an identity $m \times m$ matrix. Now, the time derivative of the storage function along the trajectories (13) under control action (14) yields:

$$\dot{V}_1(\Phi(t)) = -\Phi^{\mathsf{T}}(t)\boldsymbol{\rho}\mathrm{Sign}(\Phi(t)) + \Phi^{\mathsf{T}}(t)\chi(z, t) \quad (17)$$

where $\chi(z, t) = \mathbf{M}_4\bar{\xi}(z, t) + \mathbf{M}_5\dot{\bar{\xi}}(z, t)$, $\mathbf{M}_4 = \mathbf{K}_3\,[\mathbf{Q}_1,\ \mathbf{Q}_2]$ $+\mathbf{K}_1\left[\mathbf{R},\ \mathbf{I}_m\right]$, and $\mathbf{M}_5 = \mathbf{K}_3\left[\mathbf{R},\ \mathbf{I}_m\right]$.

From Assumption 1, we can see that

$$\|\bar{\xi}(z, t)\| \leq \delta_3,\ \left\|\dot{\bar{\xi}}(z, t)\right\| \leq \delta_4, \quad (18)$$

where $\delta_3 = |\lambda_{\max}(T)|\delta_1$, $\delta_4 = |\lambda_{\max}(T)|\delta_2$,

$$\dot{V}_1(\Phi(t)) \leq -\max\{\rho_i\}\sum_{i=1}^{n}|\Phi_i(t)| + \|\Phi(t)\chi(z, t)\| \quad (19)$$

and defining ρ_i, such that $\rho_i = \alpha_1 + \delta_1$ is guaranteed for some $0 < \alpha_1 \in \mathbb{R}$, the next statement is obtained:

$$\begin{aligned}
\dot{V}_1(\Phi(t)) &\leq -\alpha_1\sum_{i=1}^{n}|\Phi_i(t)| = -\alpha_1|\Phi(t)|\\
&\leq -\alpha_1\sqrt{2}V_1^{\frac{1}{2}}(\Phi(t)).
\end{aligned} \quad (20)$$

In this sense, the solution of the differential equation:

$$\dot{V}_1(\Phi(t)) = -\alpha_1\sqrt{2}\, V_1^{\frac{1}{2}}(\Phi(t)), \tag{21}$$

along the time interval $\tau \in [t_0, t)$ is as follows:

$$\int_{t_0}^{t} V_1^{-\frac{1}{2}}(\Phi(\tau))dV_1(\Phi(\tau)) = -\alpha_1\sqrt{2}\int_{t_0}^{t} d\tau, \tag{22}$$

and finally it yields:

$$V_1^{\frac{1}{2}}(\Phi(t)) = V_1^{\frac{1}{2}}(\Phi(t_0)) - \frac{\alpha_1}{\sqrt{2}}(t - t_0). \tag{23}$$

By using the comparison theorem, the solution of the previous differential inequality is given by:

$$V_1^{\frac{1}{2}}(\Phi(t)) \leq V_1^{\frac{1}{2}}(\Phi(t_0)) - \frac{\alpha_1}{\sqrt{2}}(t - t_0). \tag{24}$$

Note that the storage function (where it's time variation is depicted in (15)) is a positive definite function. This means that eventually as time t is increasing, the time t_r is obtained from the solution of next equation

$$0 = V_1^{\frac{1}{2}}(\Phi(t_0)) - \frac{\alpha_1}{\sqrt{2}}(t - t_0) \tag{25}$$

and the storage function arrives to the origin in time less or equal to t_r. Furthermore, it remains on it for all future time $t \geq t_r$. This means that the convergence of the sliding variable to the origin is guaranteed at the same time. □

Noticed that, after time t_r, the sliding variable $\Phi(t) = \bar{0}_m$ is satisfied, in this way it is evident that

$$\bar{0}_m = \mathbf{K}_1\varphi(t) + \mathbf{K}_2\int_{t_0}^{t}\varphi(\tau)d\tau + \mathbf{K}_3\dot{\varphi}(t), \tag{26}$$

or equivalently:

$$\bar{0}_m = \mathbf{K}_1\dot{\varphi}(t) + \mathbf{K}_2\varphi(t) + \mathbf{K}_3\ddot{\varphi}(t) \tag{27}$$

This means that:

$$\varphi(t) = -\mathbf{K}_2^{-1}\mathbf{K}_1\dot{\varphi}(t) - \mathbf{K}_2^{-1}\mathbf{K}_3\ddot{\varphi}(t)$$

$$\varphi(t) = -\mathbf{K}_2^{-1}\left\{\mathbf{K}_1\left(\left[\mathbf{R},\ \mathbf{I}_m\right]\bar{\xi}\right) - \mathbf{K}_3\left[\mathbf{Q}_1,\ \mathbf{Q}_2\right]\bar{\xi}(z,t)\right.$$

$$\left. -\mathbf{K}_3\left[\mathbf{R},\ \mathbf{I}_m\right]\dot{\bar{\xi}}(z,t) - \boldsymbol{\rho}\mathrm{Sign}(\Phi(t))\right\}$$

In this sense, for a bounded gain matrix $\lambda_{\max}(\mathbf{R}\mathbf{R}^{\intercal}) \leq \delta_5 < \infty$ the following statement is satisfied:

$$\begin{aligned}
&\|\varphi(t)\| \leq \delta_6,\ \delta_6 = \lambda_{\max}(\mathbf{K}_2^{-1})\left\{\lambda_{\max}(\mathbf{K}_1)M_1\delta_3 + M_2\right\},\\
&M_1 = \sqrt{\lambda_{\max}\left(\left[\mathbf{R}\ \mathbf{I}_m\right]^{\intercal}\left[\mathbf{R}\ \mathbf{I}_m\right]\right)},\\
&M_2 = \left(M_1\delta_3 + M_3\delta_4\right)\lambda_{\max}(\mathbf{K}_3) + \lambda_{\max}(\boldsymbol{\rho}),\\
&M_3 = \sqrt{\lambda_{\max}\left(\left[\mathbf{Q}_1\ \mathbf{Q}_2\right]^{\intercal}\left[\mathbf{Q}_1\ \mathbf{Q}_2\right]\right)}.
\end{aligned} \tag{28}$$

From the definition of the adjoint variable $\varphi(t) = z_2(t) + \mathbf{R}z_1(t)$ and Proposition 2, it can be shown that $z_2(t) = \varphi(t) - \mathbf{R}z_1(t)$ is satisfied. In this sense, from (13) the following statement is fulfilled:

$$\begin{aligned}
&\dot{z}_1(t) = \left(\mathcal{A}_{11} - \mathcal{A}_{12}\mathbf{R}\right)z_1(t) + \zeta(t),\\
&\zeta(t) = \mathcal{A}_{12}\varphi(t) + \bar{\xi}_1(z,t),\ z_1(0) = z_1^0.
\end{aligned} \tag{29}$$

where $\|\zeta(t)\| \leq \delta_6\sqrt{\lambda_{\max}(\mathcal{A}_{12}^{\intercal}\mathcal{A}_{12})} + \delta_3$. To guarantee the UUB-stability of the subsystem (29), the following proposition is provided.

Proposition 3: Under assumption of Proposition 2. Consider the storage function $V_2(z_1(t)) = z_1^{\intercal}(t)\mathbf{P}z_1(t)$, with a positive definite matrix $\mathbf{P} \in \mathbb{R}^{(n-m)\times(n-m)}$. If there exists a set of solutions $(\alpha_2, \beta, \mathbf{P}, \mathbf{R})$, where $\mathbf{R} \in \mathbb{R}^{m\times(n-m)}$ is an adjustment matrix, α_2 and ε are positive scalars, such that the following matrix inequality is fulfilled:

$$\mathbf{W} = \begin{bmatrix}\mathbf{A_5} + \alpha_2\mathbf{P} & \mathbf{P}\\ \mathbf{P} & -\varepsilon\mathbf{I}_r\end{bmatrix} < 0, \tag{30}$$

where $\mathbf{I}_r$ defines the $(n-m)\times(n-m)$ identity matrix, and $\mathbf{A_5} = \mathbf{P}(\mathcal{A}_{11} - \mathbf{R}\mathcal{A}_{12}) + (\mathcal{A}_{11}^{\intercal} - \mathcal{A}_{12}^{\intercal}\mathbf{R}^{\intercal})\mathbf{P}$, then the storage function $V_2(z_1(t))$ satisfies:

$$V_2\left(z_1(t)\right) \leq \frac{\beta}{\alpha_2} + \left\{V_2\left(z_1(t_r)\right) - \frac{\beta}{\alpha_1}\right\}\exp(-\alpha_2(t - t_r)) \tag{31}$$

where $\beta = \varepsilon(\delta + \delta_3)$, the UUB-Stability is concluded with:

$$\begin{aligned}
&b = \sqrt{\frac{\beta}{\alpha_2}\lambda_{\max}(\mathbf{P^{-1}})},\\
&T_2 = \frac{1}{\alpha_2}\ln\left\{\frac{\alpha_2 V(z_1^0) - \beta}{\beta\gamma}\right\} + \frac{\sqrt{2}}{\mathrm{trace}(\rho_{\mathbf{0}})}V_1^{\frac{1}{2}}(z_1^0) + t_0,
\end{aligned} \tag{32}$$

for small-enough constant $\zeta(t) \in \mathbb{R}^{+}$.

Proof. Calculating the time derivative of the storage function $V_2(z_1(t))$ along the trajectories (29) yields:

$$\begin{aligned}
\dot{V}_2(z_1(t)) = &\left[z_1(t)\ \zeta(t)\right]\mathbf{W}\left[z_1(t)\ \zeta(t)\right]^{\intercal}\\
&- \alpha_2 V_2(z_1(t)) + \varepsilon\|\zeta(t)\|^2.
\end{aligned} \tag{33}$$

From the properties given in (28), and under the assumption that $\mathbf{W} < 0$, the following inequality is fulfilled:

$$\dot{V}_2(z_1(t)) \leq -\alpha_2 V_2(z_1(t)) + \beta \tag{34}$$

thus, by the comparison principle, see for instance [38], [39], the solution of the differential equation

$$\dot{V}_2(z_1(t)) + \alpha_2 V_2(z_1(t)) = \beta \tag{35}$$

in the time interval $\tau \in [0, t)$ is given by the upper bound of (31). In fact, differential inequality (34) implies that Proposition 1 is satisfied, implying that (12) is fulfilled. This means that the storage function $V(z_1(t))$ is an attractive invariant set. Finally, it is clear that error function exponentially arrives into an invariant set $\Upsilon_1 = \{z_1(t) \in \mathbb{R}^n : \|z_1(t)\| \leq b, \forall\, t \geq T_2\}$. In other words, the error function arrives into an attractive ellipsoid with ellipsoid

matrix $\bar{\mathbf{P}} = \frac{\alpha}{\varepsilon}\mathbf{P}^{-1}$. From the previous inequality, it is clear that $\lim_{t\to\infty} V_2(z_1(t)) \leq \frac{\beta}{\alpha_2}$, and equation (32) is obtained. □

Remark 1: Previous result (Proof of 3), say that the ultimate bound must be reduced by increasing the parameter α_2 and decreasing ε. However, note that its ultimate bound depends of δ_6 and this one can be considerably reduced or increased from the sliding manifold tuning. In order to reduce the parameter β, select the eigenvalues of matrix $\mathbf{K}_2$ as largest as possible, and the eigenvalues of the matrices $\mathbf{K}_1$ and $\mathbf{K}_3$ small enough. Note that for larger magnitudes of $\lambda_i(\mathbf{K}_2^{-1})$, $(i = 1, \ldots, m)$, the parameter β approaches to δ_3.

Notice that in the frequency domain, the sliding surface (8) can be seen as a second order filter where the input is φ and the output is Φ with its corresponding transfer function defied as:

$$\varphi(s) = s\left(s^2\mathbf{K}_3 + s\mathbf{K}_1 + \mathbf{K}_2\right)^{-1}\Phi(s) \tag{36}$$

whose characteristic polynomial $P(s)$ is given as:

$$P(s) = \prod_{i=1}^{m}\left(s^2\mathbf{K}_{3,i} + s\mathbf{K}_{1,i} + \mathbf{K}_{2,i}\right). \tag{37}$$

Here, the i-th characteristic polynomial is associated with the i-th actuator, which should be adjusted via bode filter design, a rlocus approach or a pole allocation procedure.

Remark 2: Proposition 3 indicates that for a large α_2 and small-enough β, system trajectories arrives into an attractive ellipsoid $\mathcal{E}(0, \bar{\mathbf{P}})$. In this way, the following optimization problem

$$\min_{\mathbf{P}^{-1}}\left(\frac{\beta}{\alpha_2}\lambda_{\max}(\mathbf{P}^{-1})\right) \text{ s. t. } \begin{pmatrix} 0 < \alpha_2, 0 < \varepsilon \\ 0 < \mathbf{P}, \mathbf{W} < 0 \end{pmatrix}, \tag{38}$$

is associated to obtain the minimal size of this ellipsoid, where $\bar{\mathbf{P}} = \frac{\alpha_2}{\beta}\mathbf{P}$ is the associated ellipsoidal matrix. Thus, the maximal value of $\mathbf{P}$ under maximal value of α_2 and ε in which $\mathbf{W}$ is a negative definite matrix, means that the system trajectories are enclosed into a minimal size attractive-invariant set.

V. NUMERICAL RESULTS

A. AIRCRAFT DYNAMICS IN SUBSYSTEM REPRESENTATION

The hexarotor vehicle depicted in Figure 1 was used to illustrate the performance of the linear, nonlinear, robust and non conventional control approaches. For control purposes, certain considerations are made for the dynamics described in (2). It is assumed that the Euler angles $\phi(t)$, $\theta(t)$ and $\psi(t)$ can be considered as small values and the angular velocities on the inertial frame are equal to the velocities in the body frame. Similarly, the Coriolis terms are neglected in equation (2) and it is assumed that the attitude dynamics ($\ddot{\phi}(t)$, $\ddot{\theta}(t)$ and $\ddot{\psi}(t)$) have their own control signal ($\tau_\phi(t)$, $\tau_\theta(t)$ and $\tau_\psi(t)$), such that:

$$\begin{bmatrix}\ddot{\phi}(t)\\ \ddot{\theta}(t)\\ \ddot{\psi}(t)\end{bmatrix} \approx \begin{bmatrix}\frac{I_{z_B z_B}}{a_1}\tau_\phi(t)\\ \frac{I_{z_B z_B}}{a_1}\tau_\theta(t)\\ \frac{I_{z_B z_B}}{a_1}\tau_\psi(t)\end{bmatrix}. \tag{39}$$

We defined the state vector as $\bar{x}(t) = [\bar{x}_1(t)\ \bar{x}_2(t)\ \bar{x}_3(t)\ \bar{x}_4(t)\ \bar{x}_5(t)\ \bar{x}_6(t)\ \bar{x}_7(t)\ \bar{x}_8(t)\ \bar{x}_9(t)\ \bar{x}_{10}(t)\ \bar{x}_{11}(t)\bar{x}_{12}(t)]^\mathsf{T}$, where $\bar{x}(t)$ is the connected manifold in $\mathbb{R}^{12}$. After these considerations, the dynamical model can be represented in the form $\dot{\bar{x}}(t) = f(\bar{x}) + g(\bar{x})u(t) + \zeta(t, x)$, where $\zeta(t, x)$ is the unmodeled dynamics, as:

$$f(\bar{x}) = \begin{bmatrix}0\\ \xi_x(t)\\ 0\\ \xi_y(t)\\ 0\\ -g + \xi_z(t)\\ 0\\ \xi_\phi(t)\\ 0\\ \xi_\theta(t)\\ 0\\ \xi_\psi(t)\end{bmatrix}, u(t) = \begin{bmatrix}u_z(t)\\ \tau_\phi(t)\\ \tau_\theta(t)\\ \tau_\psi(t)\end{bmatrix},$$

and $g(\bar{x}) =$

$$\begin{bmatrix}0 & 0 & 0 & 0\\ a_6 & 0 & 0 & 0\\ 0 & 0 & 0 & 0\\ a_7 & 0 & 0 & 0\\ 0 & 0 & 0 & 0\\ \frac{1}{m}(c\bar{x}_7(t)\, c\bar{x}_9(t)) & 0 & 0 & 0\\ 0 & 0 & 0 & 0\\ 0 & \frac{I_{zz}}{a_1}\tau_\phi(t) & 0 & 0\\ 0 & 0 & 0 & 0\\ 0 & 0 & \frac{1}{I_{yy}}\tau_\theta(t) & 0\\ 0 & 0 & 0 & 0\\ 0 & 0 & 0 & \frac{I_{zz}}{a_1}\tau_\psi(t)\end{bmatrix}. \tag{40}$$

where $a_6 = \frac{1}{m}(c\bar{x}_7(t)\, s\bar{x}_9(t)\, c\bar{x}_{11}(t) + s\bar{x}_7(t)\, s\bar{x}_{11}(t))$ and $a_7 = \frac{1}{m}(c\bar{x}_7(t)\, s\bar{x}_9(t)\, s\bar{x}_{11}(t) - s\bar{x}_7(t)\, c\bar{x}_{11}(t))$. $\bar{x}_1(t)$, $\bar{x}_2(t)$ and $\bar{x}_3(t)$ define the translational positions $(x(t), y(t), z(t))$, $\bar{x}_4(t)$, $\bar{x}_5(t)$ and $\bar{x}_6(t)$ represents the rotational angles $(\phi(t), \theta(t), \psi(t))$ and $\bar{x}_7(t)$ to $\bar{x}_{12}(t)$ are their velocities, respectively. Now, consider the following feedback linearization control law:

$$u_z(t) = \frac{m}{\cos\bar{x}_7(t)\, \cos\bar{x}_9(t)}(g + \bar{u}_z(t)). \tag{41}$$

Then, substituting equation (41) in equation (40), the translational equations result as:

$$\dot{\bar{x}}_2(t) = \left(\tan\bar{x}_9(t)\cos\bar{x}_{11}(t) + \tan\bar{x}_7(t)\frac{\sin\bar{x}_{11}(t)}{\cos\bar{x}_9(t)}\right)(g+\bar{u}_z(t)) + \xi_x(t),$$
$$\dot{\bar{x}}_4(t) = \left(\tan\bar{x}_9(t)\sin\bar{x}_{11}(t) - \tan\bar{x}_7(t)\frac{\cos\bar{x}_{11}(t)}{\cos\bar{x}_9(t)}\right)(g+\bar{u}_z(t)) + \xi_y(t),$$
$$\dot{x}_6(t) = \bar{u}_z(t) + \xi_z(t). \tag{42}$$

Considering (42) and system (40), we defined the following subsystems represented as system (4):

- **Altitude subsystem**: The first subsystem corresponds to the $z(t)$ position:

$$\dot{z}(t) = A_z z(t) + \mathbf{B}_z\bar{u}_z(t) + \boldsymbol{\xi}_z(t). \tag{43}$$

- **Directional Subsystem** : The second subsystem is related to the yaw angle:

$$\dot{\boldsymbol{\psi}}(t) = A_\psi\boldsymbol{\psi}(t) + \mathbf{B}_\psi\tau_\psi(t) + \boldsymbol{\xi}_{\boldsymbol{\psi}}(t). \tag{44}$$

- **Longitudinal subsystem** : The third subsystem corresponds to the pitch angle and the x position:

$$\dot{\bar{x}}_2(t) = \left(\tan\bar{x}_9(t)\cos\bar{x}_{11}(t) + \tan\bar{x}_7(t)\frac{\sin\bar{x}_{11}(t)}{\cos\bar{x}_9(t)}\right)(g+\bar{u}_z(t)) + \xi_x(t),$$
$$\dot{\boldsymbol{\theta}}(t) = A_\theta\boldsymbol{\theta}(t) + \mathbf{B}_\theta\tau_\theta(t) + \boldsymbol{\xi}_{\boldsymbol{\theta}}(t). \tag{45}$$

- **Lateral subsystem**: The fourth subsystem is the dynamic of the y position and the roll angle:

$$\dot{\bar{x}}_4(t) = \left(\tan\bar{x}_9(t)\sin\bar{x}_{11}(t) - \tan\bar{x}_7(t)\frac{\cos\bar{x}_{11}(t)}{\cos\bar{x}_9(t)}\right)(g+\bar{u}_z(t)) + \xi_y(t),$$
$$\dot{\boldsymbol{\phi}}(t) = A_\phi\boldsymbol{\phi}(t) + \mathbf{B}_\phi\tau_\phi(t) + \boldsymbol{\xi}_{\boldsymbol{\phi}}(t). \tag{46}$$

In this way, consider the following vectors and matrices:

$$\dot{z}(t) = \begin{bmatrix}\dot{\bar{x}}_5(t)\\ \dot{\bar{x}}_6(t)\end{bmatrix}, \dot{\boldsymbol{\psi}}(t) = \begin{bmatrix}\dot{\bar{x}}_{11}(t)\\ \dot{\bar{x}}_{12}(t)\end{bmatrix}, \dot{\boldsymbol{\theta}}(t) = \begin{bmatrix}\dot{\bar{x}}_9(t)\\ \dot{\bar{x}}_{10}(t)\end{bmatrix},$$
$$\dot{\boldsymbol{\phi}}(t) = \begin{bmatrix}\dot{\bar{x}}_7(t)\\ \dot{\bar{x}}_8(t)\end{bmatrix}, \mathbf{A}_i = \begin{bmatrix}0 & 1\\ 0 & 0\end{bmatrix}, \mathbf{B}_z = \begin{bmatrix}0\\ 1\end{bmatrix},$$
$$\mathbf{B}_j = \begin{bmatrix}0\\ \frac{I_{zz}}{a_1}\end{bmatrix}, \mathbf{B}_\theta = \begin{bmatrix}0\\ \frac{1}{I_{yy}}\end{bmatrix}, \boldsymbol{\xi}_i(t) = \begin{bmatrix}0\\ \xi_i(t)\end{bmatrix}, \boldsymbol{\phi}(t) = \begin{bmatrix}\bar{x}_7(t)\\ \bar{x}_8(t)\end{bmatrix}$$
$$z(t) = \begin{bmatrix}\bar{x}_5(t)\\ \bar{x}_6(t)\end{bmatrix}, \boldsymbol{\psi}(t) = \begin{bmatrix}\bar{x}_{11}(t)\\ \bar{x}_{12}(t)\end{bmatrix}, \boldsymbol{\theta}(t) = \begin{bmatrix}\bar{x}_9(t)\\ \bar{x}_{10}(t)\end{bmatrix},$$

with $i = z(t), \phi(t), \theta(t), \psi(t)$ and $j = \phi(t), \psi(t)$.

Remark 3: In order to control the translational movements in $x(t)$ and $y(t)$, we defined virtual controllers in the numerical results presented below. These controllers have the structure of a proportional-derivative control and they are designed as $\ddot{e}_x(t) = -k_1e_x(t) - k_2\dot{e}_x(t)$ and $\ddot{e}_y(t) = -k_3e_y(t) - k_4\dot{e}_y(t)$, respectively, where k_1, k_2, k_3, k_4 are positive constant gains and $e_x(t) = \bar{x}_1(t) - x_{\text{ref}}$, $e_y(t) = \bar{x}_3(t) - y_{\text{ref}}$ are the corresponding tracking errors of $x(t)$ and $y(t)$. Notice that, from equation (45), $x(t)$ can be controlled by manipulating θ, then, defining $e_\theta = \bar{x}_9 - \theta_{\text{ref}}$ and, through mathematical manipulations, the form of the reference value for theta is given by:

$$\theta_{\text{ref}} = \arctan\left\{\left(\frac{-k_1e_x(t) - k_2\dot{e}_x(t) + \ddot{x}_{\text{ref}}}{g+\bar{u}_z(t)} - a_8\right)\frac{1}{\cos\bar{x}_{11}(t)}\right\},$$
$$\text{with } a_8 = \tan\bar{x}_7(t)\frac{\sin\bar{x}_{11}(t)}{\cos\bar{x}_9(t)}. \tag{47}$$

Similarly, from equation (46), $y(t)$ can be controlled by $\phi(t)$. Defining $e_\phi(t) = \bar{x}_7(t) - \phi_{\text{ref}}$, the structure of the reference value for $\phi(t)$ is given by:

$$\phi_{\text{ref}} = \arctan\left\{\left(\frac{k_3e_y(t) + k_4\dot{e}_y(t) - \ddot{y}_{\text{ref}}}{g+\bar{u}_z(t)} + a_9\right)\frac{\cos\bar{x}_9(t)}{\cos\bar{x}_{11}(t)}\right\}.$$
$$\text{with } a_9 = \tan\bar{x}_9(t)\sin\bar{x}_{11}(t). \tag{48}$$

TABLE 1. System parameters description.

Description	Notation	Value	Units
UAV mass	m	3.091	kg
Inertia in $x_B(t)$-axis	$I_{x_Bx_B}$	0.5059	kgm^2
Inertia in $x_B(t) - y_B(t)$-axis	$I_{x_By_B}$ or $I_{y_Bx_B}$	0	kgm^2
Inertia in $x_B(t) - z_B(t)$-axis	$I_{z_Bx_B}$ or I_{xz}	-0.0910	kgm^2
Inertia in $y_B(t)$-axis	$I_{y_By_B}$	0.4119	kgm^2
Inertia in $y_B(t) - z_B(t)$-axis	$I_{z_By_B}$ or $I_{y_Bz_B}$	0	kgm^2
Inertia in $z_B(t)$-axis	$I_{z_Bz_B}$	0.7822	kgm^2
Gravity constant	g	9.81	$\frac{m}{s^2}$

B. NUMERICAL RESULTS

In order to demonstrate the effectiveness of the robust controller (RC) described in Section IV, we conducted trajectory tracking simulations by using MatLab-2020Ra and multiple Simulink toolboxes, as well as the Bogacki-Shampine method with a sample time of $h_t = 0.001$ seconds.

The mission profile for every simulation scenario was defined by considering the UAV dynamics given in equation (2) and the considerations presented in Section V-A. The system parameters used in the simulations are given in Table 1. These values were obtained through the inertia and angular moment concepts, as well as the characteristics of the aircraft (lengths and mass). For all instances studied, the simulation time was set as $t \in [0, 100]$ seconds. In order to track a given trajectory for the translational dynamics ($x(t)$, $y(t)$, $z(t)$) and to keep the rotational dynamics ($\phi(t)$, $\theta(t)$, $\psi(t)$) around the origin, the desired trajectories are given in a three dimensional space ($x(t)$, $y(t)$, $z(t)$) by using the parametric equations shown in Table 2.

The designed trajectory consists of a smooth transition in speed changes during the mission. The ω term represents the frequency of the trigonometric functions used to generate the desired trajectories. The initial conditions were defined as

TABLE 2. Characteristics of the desired trajectory. $b_1 = 3.5$, $b_2 = 0.5$, $c_1 = 2$ and $\omega = 5Hz$. $c_2 = 2b_2 - 2\,b_2\cos(t/w)$, $c_3 = (b_1 + b_2)/(1 + \exp^{-0.9(t-5)})$, $c_4 = c_1 - c_1\cos(t/w)$.

Time t (s)	x_{ref}	y_{ref}	z_{ref}
$[0, \omega\pi)$	$b_1 + b_2$	c_1	c_3
$[\omega\pi, 2\omega\pi)$	$b_1 + b_2$	$-c_1\cos(t/w)$	$b_1 + 0.3$
$[2\omega\pi, 3\omega\pi)$	$b_2 + b_1\cos(t/w)$	$-a_1$	$b_1 + 0.3$
$[3\omega\pi, 4\omega\pi)$	$-b_1 + b_2$	$c_1\cos(t/w)$	$b_1 + 0.3$
$[4\omega\pi, 5\omega\pi)$	$b_2 - b_1\cos(t/w)$	c_1	$b_1 + 0.3$
$[5\omega\pi, 100)$	$c_1 - c_1\cos(t/w)$	c_2	c_4

$\bar{x}_0 = [4, 2, 0.02, 0.05, 0.03, 0.05, 0, 0, 0, 0, 0, 0]^\intercal$. We used the following disturbances for the translational and rotational dynamics of the underactuated system:

$$\begin{aligned}&\Delta(t) = \\ &[0\ \ 0.1\,c(0.1t)\ \ 0\ \ 0.1\,c(0.1t)\ \ 0\ \ 0.1\,c(3.3t)\ \ 0 \\ &0.05\,c(12.54*t)\ \ 0\ \ 0.05\,c(12.54t)\ \ 0\ \ 0.1\,c(0.1t)]^\intercal, \quad (49)\end{aligned}$$

where $c(*)$ stands for $\cos(*)$. Similarly, we used the following disturbances in the control signals: for $\bar{u}_z(t)$ a sawtooth function with an amplitude of 1.2 and a frequency of 1.5 Hz, for $\tau_\psi(t)$, $\tau_\theta(t)$ and $\tau_\phi(t)$ a random function with an amplitude of 1.2 and a frequency of 2 Hz. For the robust control, the matrix that transforms the dynamics in the form given in (4) to the representation given in (7) is given as:

$$\mathbf{T_h} = \begin{bmatrix} -1 & 0 \\ 0 & 1 \end{bmatrix}, \quad \text{for } z \text{ subsystem } \mathbf{T_z} = \begin{bmatrix} -1 & 0 \\ 0 & 100 \end{bmatrix} \quad (50)$$

where $h = \phi(t), \theta(t), \psi(t)$.

In general, the sliding surface (8) for each subsystem $i = \{z(t),\ \phi(t),\ \theta(t),\ \psi(t)\}$ is obtained as follows:

$$\Phi_i(t) = \mathbf{K}_{1i}\varphi_i(t) + \mathbf{K}_{2i}\int_{t_0}^{t}\varphi_i(\tau)d\tau + \mathbf{K}_{3i}\dot{\varphi}_i(t), \quad (51)$$

with $\mathbf{K}_{1z} = 0.03118$, $\mathbf{K}_{2z} = 0.02348$, $\mathbf{K}_{3z} = 0.0188$, $\mathbf{K}_{1\phi} = 6.236$, $\mathbf{K}_{2\phi} = 2.348$, $\mathbf{K}_{3\phi} = 0.0376$, $\mathbf{K}_{1\theta} = 1.559$, $\mathbf{K}_{2\theta} = 0.2348$, $\mathbf{K}_{3\theta} = 0.0376$, $\mathbf{K}_{1\psi} = 0.3118$, $\mathbf{K}_{2\psi} = 0.2348$, $\mathbf{K}_{3\psi} = 0.188$. These gains were obtained heuristically by conducting several simulations.

Using the MatLab Yalmip-CVX toolbox, the above numerical procedure gives the following set of numerical solutions

$$\begin{aligned}&\alpha_1 = 0.35,\ \varepsilon = 2.9\times10^{-5}, \\ &\mathbf{X} = 1.319\times10^4,\ \mathbf{Y} = -2.209\times10^4,\ \mathbf{R} = -1.674, \\ &\quad \text{for } \phi(t), \theta(t) \text{ and } \psi(t). \\ &\mathbf{X}_z = 1.319\times10^4, \mathbf{Y}_z = -2.209\times10^6, \mathbf{R}_z = -167.487, \\ &\quad \text{for } z(t). \quad (52)\end{aligned}$$

The robust control action associated with the UAV dynamics is given as:

$$\begin{aligned}\dot{u}(t) = &\\ &-\mathcal{B}_{i2}^{-1}\mathbf{K}_{3i}^{-1}\{(\mathbf{K}_{3i}\{\mathbf{Q}_{i1}\mathcal{A}_{i11}+\mathbf{Q}_{i2}\mathcal{A}_{i21}\}+\mathbf{K}_{1i}\mathbf{Q}_{i1})\,z_{i1}(t) \\ &+\ (\mathbf{K}_{3i}\{\mathbf{Q}_{i1}\mathcal{A}_{i12}+\mathbf{Q}_{i2}\mathcal{A}_{i22}\}+\mathbf{K}_{2i}+\mathbf{K}_{1i}\mathbf{Q}_{i2})\,z_{i2}(t) \\ &+\ (\mathbf{K}_{3i}\mathbf{Q}_{i2}\mathcal{B}_{i2}+\mathbf{K}_{i1}\mathcal{B}_{i2})\,u(t) + \boldsymbol{\rho}_i\text{Sign}(\Phi_i(t))\}. \\ &\quad (53)\end{aligned}$$

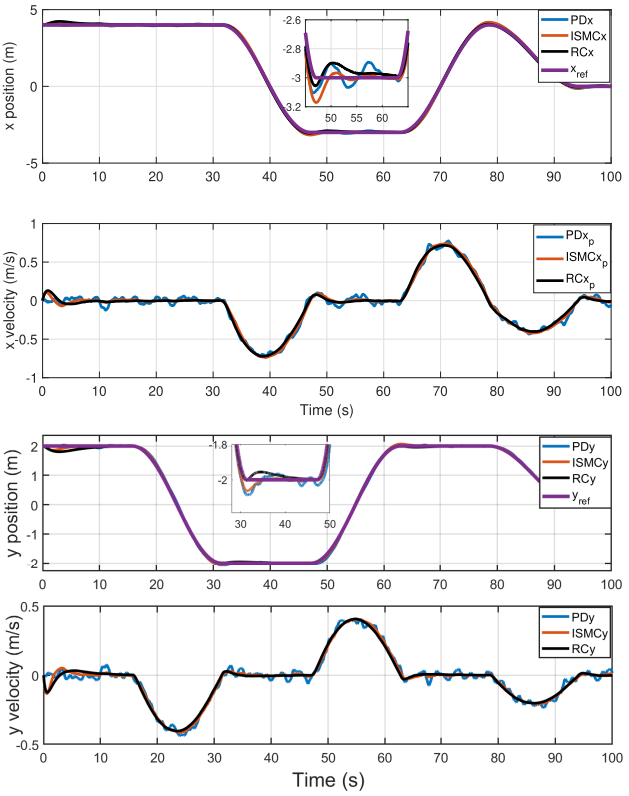

FIGURE 2. Positions and velocities of the $x(t)$ and $y(t)$ dynamics obtained from the implementation of the PD, ISM and Robust controllers.

For the conducted tests we used:

$$\begin{aligned}&\mathcal{A}_z = \begin{bmatrix} 0 & -1 \\ 0 & 0 \end{bmatrix}\ \mathcal{A}_h = \begin{bmatrix} 0 & -0.01 \\ 0 & 0 \end{bmatrix},\ \mathcal{B}_z = \begin{bmatrix} 0 \\ 1 \end{bmatrix} \\ &\mathcal{B}_h = \begin{bmatrix} 0 \\ 1\times10^4 \end{bmatrix}, \mathbf{Q}_{z2} = 1.6749,\ \mathbf{Q}_{h2} = 1.6748, \\ &\boldsymbol{\rho}_z = 7.95455\ \ \boldsymbol{\rho}_h = 0.0795.\end{aligned}$$

The values for $\mathbf{K}_{1i}$, $\mathbf{K}_{2i}$ and $\mathbf{K}_{3i}$ have already been defined previously. For considered $\gamma = 0.0001$, the ultimate bound is obtained as $b = 0.0010$. Thus, the system's trajectories arrive to its ultimate bound in time $T = 2.046$ seconds.

In order to compare the designed robust control, traditional PD control and integral sliding mode control (ISMC) were tested. The simulation parameters for the last two are described below. Figures 2 to 4, shown the simulation results associated to system under representation (7). The blue, orange, and black lines show the system response for the controllers PD, ISMC and RC, respectively. The figures are divided into subfigures, the upper ones correspond to the positions and the lower ones are related to the speeds.

The design of PD [40] controller is

$$u(t) = k_p\bar{x}(t) + k_d\dot{\bar{x}}(t), \quad (54)$$

where k_p and k_d are control gains. The control inputs for the tests performed are $u_{\bar{u}_z} = k_{pz}e_z + k_{dz}\dot{e}_z$, $u_\phi = k_{p\phi}e_\phi + k_{d\phi}\dot{e}_\phi$, $u_\theta = k_{p\theta}e_\theta + k_{d\theta}\dot{e}_\theta$ and $u_\psi = k_{p\psi}e_\psi + k_{d\psi}\dot{e}_\psi$. The tuning of

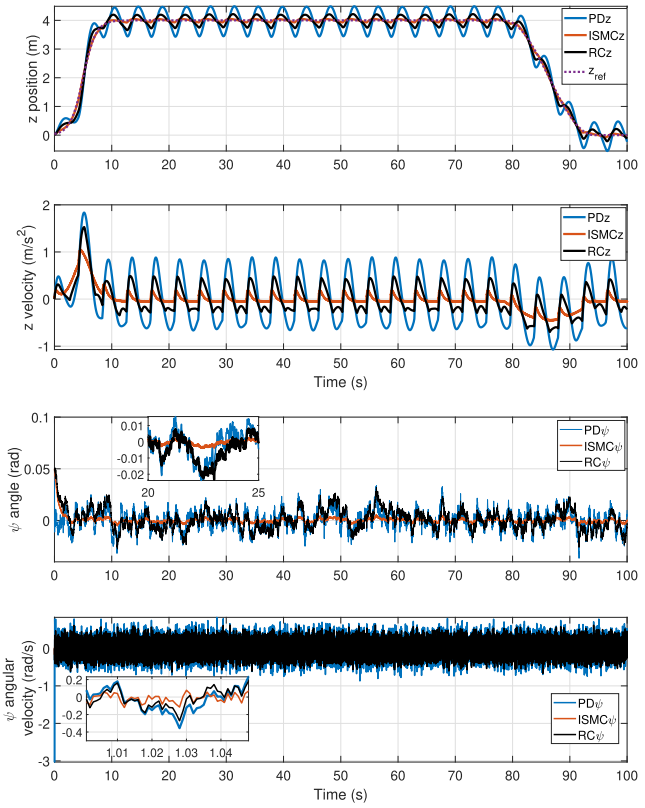

FIGURE 3. $z(t)$ position, $\psi(t)$ angular position and velocities with PD, ISMC, and Robust controller.

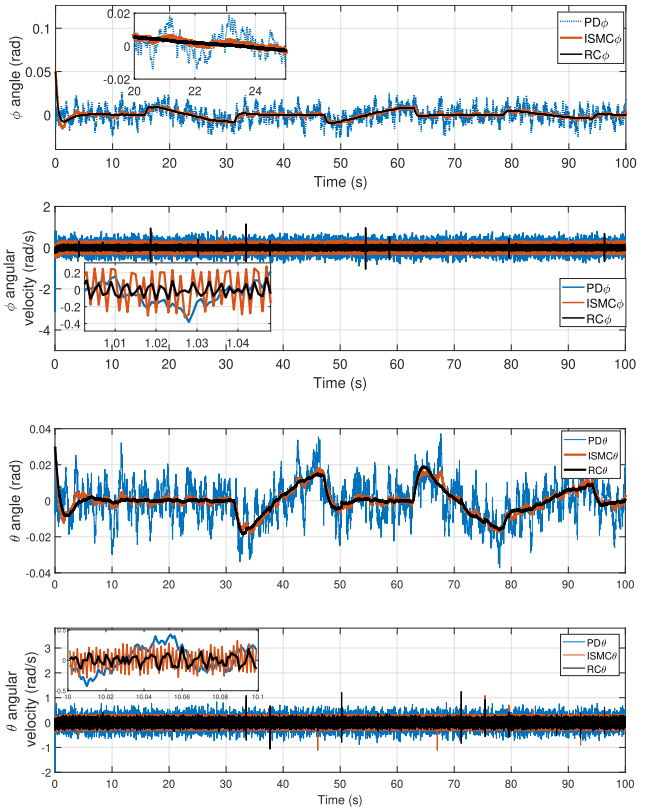

FIGURE 4. Attitude ($\phi(t)$, $\theta(t)$) and angular velocities with PD, ISMC, and Robust controller.

the gains was done using the simulink PID toolbox, however, through a fine tuning with $k_{pz} = 2$, $k_{dz} = 1$, $k_{p\phi} = 2.5$, $k_{d\phi} = 1$, $k_{p\theta} = 2.5$, $k_{d\theta} = 1$, $k_{p\psi} = 2.5$, and $k_{d\psi} = 1$ were the chosen values.

On the other hand, an integral sliding mode control was designed as it is present in [15]. To this end, system 4 was considered. The sliding surface is defined by

$$\sigma(\bar{x}(t)) = G(\bar{x}(t) - \bar{x}(0)) - G\int_o^t (A\bar{x}(\tau) + Bu_0(\tau))d\tau, \tag{55}$$

with $G \in \mathbb{R}^{m\times n}$ and $\det(GB) \neq 0$ is satisfied. The integral sliding mode control is given by

$$u(t) = u_0(t) + u_1(t), \quad u(t) \in U(t) \in \mathbb{R}^m, \tag{56}$$

where $u_0(t)$ is a nominal controller and $u_1(t)$ is designed to compensate unmatched disturbances. The design of $u_0(t)$ is just used to stabilize the nominal system and was the PD controller previously mentioned. The auxiliary control on ISMC is considered as

$$u_1(t) = -(GB)^T \rho(t,\bar{x})\ \text{sign}(\sigma(\bar{x}(t))) \tag{57}$$

where $\rho(t,x) \geq \| \xi^+(t,x) \|$ and $\xi^+(t,x)$ is upper bound for ξ. The values used for each subsystem in the simulations are $G_z = \begin{bmatrix}0.15 & 0.15\end{bmatrix}$, $G_\phi = \begin{bmatrix}0.11 & 0.11\end{bmatrix}$, $G_\theta = \begin{bmatrix}0.11 & 0.11\end{bmatrix}$,

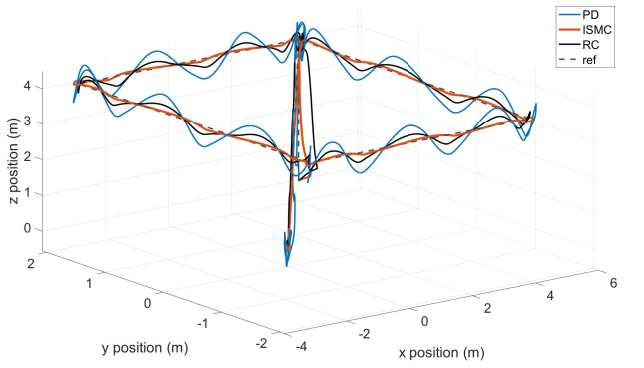

FIGURE 5. 3-Dimensional Figure shows vehicle trajectories with PD, ISMC, robust controller, and reference of $x(t)$, $y(t)$ and $z(t)$ dynamics.

$G_\psi = \begin{bmatrix}0.11 & 0.11\end{bmatrix}$ $\rho_z = 100$, $\rho_\phi = 100$, $\rho_\theta = 100$ and $\rho_\psi = 100$.

The translational performance of the UAV, in the $x(t)$, $y(t)$, $z(t)$ space is shown in Figure 5. In addition, Figure 6 presents the control signal for the strategies during trajectory tracking.

The ISMC has a good performance compared to the other two controllers while the system is subjected to disturbances. But one disadvantage is the high energy consumption of this one. Also, the conclusion of which control strategy has the highest performance is presented in an analysis based on the error response. The analysis results are presented in Table 3 in terms of the translational dynamics. The absolute error

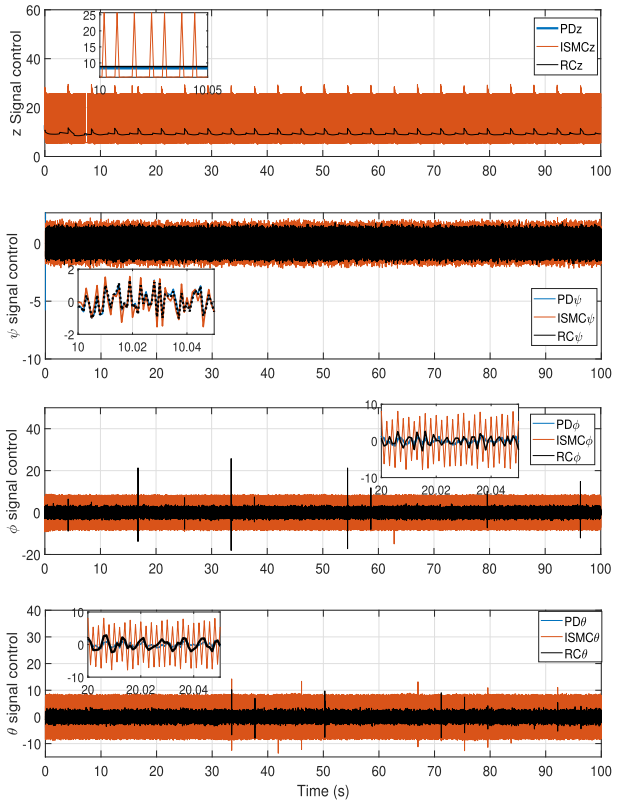

FIGURE 6. Signal controls of $z(t)$, $\psi(t)$, $\phi(t)$ and $\theta(t)$ dynamics.

TABLE 3. Errors comparative in the trajectory tracking of the UAV.

Controlller	IAE	ITAE	ISE	ITSE
PD	64.6069	3248.7833	43.1353	2170.9200
RC	29.8830	1442.2882	9.8079	450.7579
ISMC	11.2153	571.4193	1.5070	77.0232

(for IAE and ITAE) illustrates which control algorithm has a better performance compared to each other. The control strategy that shows the best performance is the ISMC with respect to the RC and PD controller, as well as, the robust control shows values similar to the ISM controller. Also, the analysis exhibit the energy consumption of each controller and demonstrate the higher consumption energy is for the ISMC to reject disturbances.

The analysis of the energy consumption is defined by:

$$E_T = \int_0^t u(\tau)^\intercal u(\tau) d\tau. \tag{58}$$

The results demonstrate that the energy consumed during the flight mission for the designed robust controller was $E_{T_{RC}} = 9041.6110\ N^2m^2s$, while for the proportional derivative controller was $E_{T_{PD}} = 8905.4839\ N^2m^2s$, and for the integral sliding mode control was $E_{T_{ISMC}} = 28262.3408\ N^2m^2s$. The PD control presents the best performance in terms of energy consumption, due to it's structure. However, the value of the energy consumed by the robust controller is not too far from the obtained with the PD controller.

VI. CONCLUSION

In this paper, a robust control which reduces the uncertain and disturbance effects of a six-rotor aircraft was designed. By solving a specific linear matrix inequality related with a sliding mode control, the Attractive Ellipsoid Method helped to conclude the Ultimate Uniform Bounded Stability around the trivial solution of the system. Furthermore, the tests with the six-rotor underactuated system exposed the effectiveness of the robust control algorithm designed here. The control showed that by increasing the perturbation magnitude, the control also augments and guarantees the same behavior in the translational dynamics. Despite, from the comparative study in terms of the IAE, ITAE, ISE and ITSE criteria, the ISMC demonstrated to have a better performance with respect to the obtained with the PD and RC controllers, it was the robust controller which exhibited a better performance in terms of energy consumption.

A. ABBREVIATIONS AND ACRONYMS

The following abbreviations are used in this manuscript:

UAV	unmanned Aerial Vehicle.
SMC	Sliding Mode Control.
AEM	Attractive ellipsoid Method.
RC	Robust Control.
UUB	Ultimately Uniformly Bounded.
PD	Proportional Derivative (control).
ISMC	Integral Sliding Mode Control.
ITAE	Integral Time Absolute Error.
ISE	Integral Square Error.
ITSE	Integral Time Square Error.
PID	Proportional Integral Derivative.

REFERENCES

[1] D. Chen and Y. Zhang, "Robust zeroing neural-dynamics and its time-varying disturbances suppression model applied to mobile robot manipulators," *IEEE Trans. Neural Netw. Learn. Syst.*, vol. 29, no. 9, pp. 4385–4397, Sep. 2018.

[2] Y.-S. Ha and S. Yuta, "Trajectory tracking control for navigation of the inverse pendulum type self-contained mobile robot," *Robot. Auto. Syst.*, vol. 17, nos. 1–2, pp. 65–80, Apr. 1996.

[3] S. Jeong and T. Hayashi, "Development of a wheeled inverted pendulum mobile platform with a four-bar parallel mechanism," *Adv. Robot.*, vol. 32, no. 4, pp. 191–201, Feb. 2018.

[4] C. He, K. Huang, X. Chen, Y. Zhang, and H. Zhao, "Transportation control of cooperative double-wheel inverted pendulum robots adopting udwadia-control approach," *Nonlinear Dyn.*, vol. 91, no. 4, pp. 2789–2802, Mar. 2018.

[5] T. Takei, R. Imamura, and S. Yuta, "Baggage transportation and navigation by a wheeled inverted pendulum mobile robot," *IEEE Trans. Ind. Electron.*, vol. 56, no. 10, pp. 3985–3994, Oct. 2009.

[6] I. Fantoni and R. Lozano, *Non-Linear Control for Underactuated Mechanical Systems*. Cham, Switzerland: Springer, 2002.

[7] T. Johnson, S. Zhou, W. Cheah, W. Mansell, R. Young, and S. Watson, "Implementation of a perceptual controller for an inverted pendulum robot," *J. Intell. Robotic Syst.*, vol. 99, nos. 3–4, pp. 683–692, Sep. 2020.

[8] R. Mondal, A. Chakraborty, J. Dey, and S. Halder, "Optimal fractional order PI$^\lambda$D$^\mu$ controller for stabilization of cart-inverted pendulum system: Experimental results," *Asian J. Control*, vol. 22, no. 3, pp. 1345–1359, 2020.

[9] A. K. Bhatia, J. Jiang, Z. Zhen, N. Ahmed, and A. Rohra, "Projection modification based robust adaptive backstepping control for multipurpose quadcopter UAV," *IEEE Access*, vol. 7, pp. 154121–154130, 2019.

[10] L. R García, A. Dzul, R. E. Lozano, and C. Pégard, *Quad Rotorcraft Control Vision-Based Hovering and Navigation* London, U.K.: Springer, 2013.
[11] Z. Cai, S. Zhang, and X. Jing, "Model predictive controller for quadcopter trajectory tracking based on feedback linearization," *IEEE Access*, vol. 9, pp. 162909–162918, 2021.
[12] M. S. Esmail, M. H. Merzban, A. A. M. Khalaf, H. F. A. Hamed, and A. I. Hussein, "Attitude and altitude tracking controller for quadcopter dynamical systems," *IEEE Access*, vol. 10, pp. 53344–53358, 2022.
[13] P. Ordaz, M. Ordaz, C. Cuvas, and O. Santos, "Reduction of matched and unmatched uncertainties for a class of nonlinear perturbed systems via robust control," *Int. J. Robust Nonlinear Control*, vol. 29, no. 8, pp. 2510–2524, May 2019.
[14] A. Poznyak, A. Polyakov, and V. Azhmyakov, *Attractive Ellipsoids in Robust Control*. Cham, Switzerland: Springer, 2014.
[15] Y. Shtessel, C. Edwards, L. Fridman, and A. Levant, *Sliding Mode Control and Observation*. Cham, Switzerland: Springer, 2014.
[16] V. I. Utkin and H.-C. Chang, "Sliding mode control on electro-mechanical systems," *Math. Problems Eng.*, vol. 8, nos. 4–5, pp. 451–473, 2002.
[17] H. Lee and V. I. Utkin, "Chattering suppression methods in sliding mode control systems," *Annu. Rev. Control*, vol. 31, no. 2, pp. 179–188, Jan. 2007.
[18] V. Utkin and H. Lee, "Chattering problem in sliding mode control systems," *IFAC Proc. Volumes*, vol. 39, no. 5, p. 1, 2006.
[19] S. Kasera, A. Kumar, and L. B. Prasad, "Analysis of chattering free improved sliding mode control," in *Proc. Int. Conf. Innov. Inf., Embedded Commun. Syst. (ICIIECS)*, Mar. 2017, pp. 1–6.
[20] Y. Orlov, L. Aguilar, and J. C. Cadiou, "Switched chattering control vs. Backlash/friction phenomena in electrical servo-motors," *Int. J. Control*, vol. 76, nos. 9–10, pp. 959–967, Jan. 2003.
[21] O. García, P. Ordaz, O.-J. Santos-Sánchez, S. Salazar, and R. Lozano, "Backstepping and robust control for a quadrotor in outdoors environments: An experimental approach," *IEEE Access*, vol. 7, pp. 40636–40648, 2019.
[22] R. Cui, X. Zhang, and D. Cui, "Adaptive sliding-mode attitude control for autonomous underwater vehicles with input nonlinearities," *Ocean Eng.*, vol. 123, pp. 45–54, Sep. 2016.
[23] O. Mofid, S. Mobayen, and W.-K. Wong, "Adaptive terminal sliding mode control for attitude and position tracking control of quadrotor UAVs in the existence of external disturbance," *IEEE Access*, vol. 9, pp. 3428–3440, 2021.
[24] J. Davila and A. Poznyak, "Dynamic sliding mode control design using attracting ellipsoid method," *Automatica*, vol. 47, no. 7, pp. 1467–1472, Jul. 2011.
[25] A. Eltayeb, M. F. Rahmat, M. A. M. Basri, M. A. M. Eltoum, and M. S. Mahmoud, "Integral adaptive sliding mode control for quadcopter UAV under variable payload and disturbance," *IEEE Access*, vol. 10, pp. 94754–94764, 2022.
[26] A. Pisano, M. Tanelli, and A. Ferrara, "Switched/time-based adaptation for second-order sliding mode control," *Automatica*, vol. 64, pp. 126–132, Feb. 2016.
[27] A. Polyakov and A. Poznyak, "Invariant ellipsoid method for minimization of unmatched disturbances effects in sliding mode control," *Automatica*, vol. 47, no. 7, pp. 1450–1454, Jul. 2011.
[28] V. I. Utkin and A. S. Poznyak, "Adaptive sliding mode control with application to super-twist algorithm: Equivalent control method," *Automatica*, vol. 49, no. 1, pp. 39–47, Jan. 2013.
[29] A. Eltayeb, M. F. Rahmat, M. A. M. Basri, M. A. M. Eltoum, and S. El-Ferik, "An improved design of an adaptive sliding mode controller for chattering attenuation and trajectory tracking of the quadcopter UAV," *IEEE Access*, vol. 8, pp. 205968–205979, 2020.
[30] S. A. Nazin, B. T. Polyak, and M. V. Topunov, "Rejection of bounded exogenous disturbances by the method of invariant ellipsoids," *Autom. Remote Control*, vol. 68, no. 3, pp. 467–486, Mar. 2007.
[31] Z. Lin, "Low gain and low-and-high gain feedback: A review and some recent results," in *Proc. Chin. Control Decis. Conf.*, Jun. 2009, pp. 52–61.
[32] K. V. Rao and A. T. Mathew, "Dynamic modeling and control of a hexacopter using PID and back stepping controllers," in *Proc. Int. Conf. Power, Signals, Control Comput. (EPSCICON)*, Jan. 2018, pp. 1–7.
[33] B. Zhao and D. Yue, "Nonlinear robust attitude control development for a hexarotor unmanned aerial vehicle," in *Proc. 33rd Youth Academic Annu. Conf. Chin. Assoc. Autom. (YAC)*, May 2018, pp. 191–195.
[34] D. Shawky, C. Yao, and K. Janschek, "Nonlinear model predictive control for trajectory tracking of a hexarotor with actively tiltable propellers," in *Proc. 7th Int. Conf. Autom., Robot. Appl. (ICARA)*, Feb. 2021, pp. 128–134.
[35] E. S. Espinoza, O. Garcia, I. Lugo, P. Ordaz, A. Malo, and R. Lozano, "Modeling and sliding mode control of a micro helicopter-airplane system," *J. Intell. Robotic Syst.*, vol. 73, nos. 1–4, pp. 469–486, Jan. 2014.
[36] G. E. M. Abro, S. A. B. M. Zulkifli, and V. S. Asirvadam, "Performance evaluation of Newton Euler & quaternion mathematics-based dynamic models for an underactuated quadrotor UAV," in *Proc. 11th IEEE Int. Conf. Control Syst., Comput. Eng. (ICCSCE)*, Aug. 2021, pp. 142–147.
[37] R. Jia and X. Zong, "Quadrotor UAV trajectory tracking control based on ASMC and improved ARDC," in *Proc. Chin. Autom. Congr. (CAC)*, Nov. 2020, pp. 6078–6083.
[38] W. M. Haddad and V. Chellaboina. *Nonlinear Dynamical Systems and Control: A Lyapunov-Based Approach*. Princeton, NJ, USA: Princeton Univ. Press, 2011.
[39] H. K. Khalil and J. W. Grizzle, *Nonlinear Systems*, vol. 3. Upper Saddle River, NJ, USA: Prentice-Hall, 2002.
[40] K. J. Åström and H. Tore, *Control PID Avanzado*. London, U.K.: Pearson, 2009.

JOVANI ORTEGA VENTURA received the bachelor's degree in electronic and telecommunications engineering and the M.Sc. degree in automatization and control from the Autonomous University of the State of Hidalgo, Hidalgo, Mexico, in 2015 and 2018, respectively, where he is currently pursuing the Ph.D. degree. His thesis is on adaptive navigation of an unmanned hybrid aerial vehicle for volcanic monitoring applications. His research interests include nonlinear control of electromechanical systems, sliding mode control, and unmanned aerial vehicles (UAV's).

DANIEL BENITEZ MORALES received the bachelor's degree in mechatronics from the Polytechnic University of Pachuca and the M.Sc. degree in automatization and control from the Autonomous University of the State of Hidalgo, Hidalgo, Mexico, where he is currently pursuing the Ph.D. degree. His research interests include UAVs and UGV applications, self-driving cars, and control of this kind of vehicle.

JESUS P. ORDAZ OLIVER received the bachelor's degree in electronic and telecommunications engineering and the M.Sc. degree in automatic control from the Autonomous University of the State of Hidalgo, Hidalgo, Mexico, in 2004 and 2007, respectively, and the Ph.D. degree in automatic control from CINVESTAV, Mexico City, in 2012. He is currently with the Autonomous University of the State of Hidalgo. His research interests include nonlinear control systems, robust control, adaptive control, system identification, and observation.

EDUARDO S. ESPINOZA QUESADA (Senior Member, IEEE) received the Ph.D. degree in automatic control from the Center for Research and Advanced Studies, National Polytechnic Institute, Mexico, in 2013. He was a Postdoctoral Researcher with the Nevada Advance Autonomous Systems Innovation Center, University of Nevada, Reno, NV, USA, in 2016. He is currently a Professor with UMI-LAFMIA, Mexico. His research interests include UASs applications and resilient strategies for design and control of eVTOL aircraft.